High-precision direct measurements of $^{13}CH_4/^{12}CH_4$ and $^{12}CH_3D/^{12}CH_4$ ratios in atmospheric methane sources by means of a long-path tunable diode laser absorption spectrometer

Peter Bergamaschi, Michael Schupp, and Geoffrey W. Harris

Measurements of $^{13}CH_4/^{12}CH_4$ and $^{12}CH_3D/^{12}CH_4$ ratios in atmospheric methane (CH_4) sources provide important information about the global CH_4 budget as well as about CH_4 production and consumption processes occurring within the various sources. As an alternative to the conventional mass spectrometer (MS) technique, which requires conversion of CH_4 to CO_2 and H_2, we have developed a tunable diode laser absorption spectrometer (TDLAS), which permits rapid direct measurements of the $^{13}CH_4/^{12}CH_4$ and $^{12}CH_3D/^{12}CH_4$ ratios. An intercomparison between TDLAS and MS techniques for samples from natural wetlands, landfills, and natural gas sources resulted in a mean deviation of $\Delta\delta^{13}C = 0.44‰$ and $\Delta\delta D = 5.1‰$. In the present system the minimum mixing ratios required are 50 parts in 10^6 by volume (ppmv) CH_4 (sample size 2 μmol CH_4) for direct $\delta^{13}C$ measurements and 2000 ppmv (sample size 80 μmol CH_4) for direct δD measurements. These mixing-ratio limits are adequate for most CH_4 source characterization studies without requiring sample preconcentration.

Key words: Tunable diode laser, laser spectroscopy, $^{13}CH_4/^{12}CH_4$, $^{12}CH_3D/^{12}CH_4$, isotope ratio, atmospheric CH_4.

1. Introduction

Recent concern about the increasing CH_4 concentration in the atmosphere[1–3] has arisen because of the contribution of CH_4 to global warming[4] as well as its complex feedback mechanisms in tropospheric and stratospheric chemistry.[4,5] Isotope measurements are an important tool in establishing the global atmospheric CH_4 budget.[6,7] For example, $^{14}CH_4$ measurements have been used to estimate the contribution of fossil sources such as natural gas and methane from coal mining or from the oil industry.[7–9] In contrast the stable isotope ratios, $^{13}CH_4/^{12}CH_4$ and $^{12}CH_3D/^{12}CH_4$, are determined by the different CH_4-production processes, i.e., (a) biogenic CH_4 production by acetate fermentation or CO_2 reduction in strictly anaerobic environments, (b) thermogenic production (at high temperatures), and (c) incomplete combustion of biomass or fossil fuels.[10] The $\delta^{13}C$–δD signatures[11] for the three CH_4-production processes are clearly distinguishable, and the two biogenic CH_4-production pathways, acetate fermentation and CO_2 reduction, can be further differentiated by an inverse $\delta^{13}C/\delta D$ correlation ($\Delta\delta D/\Delta\delta^{13}C < 0$).[14–16]

For many biogenic CH_4 sources, the CH_4 flux into the atmosphere is reduced by partial bacterial oxidation of the CH_4, which causes an enrichment of both the $\delta^{13}C$ and the δD values ($\Delta\delta D/\Delta\delta^{13}C = 3–14$).[17–21] Further effects modifying the isotopic signatures are the gradual isotopic enrichment of residual organic material in the course of degradation ($\Delta\delta D/\Delta\delta^{13}C = 0–1$)[19] and molecular diffusion, which may alter isotope signatures of natural gases on geological time scales[22] ($\Delta\delta D/\Delta\delta^{13}C = 1$).[21] Thus parallel $\delta^{13}C$ and δD measurements allow conclusions to be drawn about the production, consumption, and transport of CH_4.

Until now $\delta^{13}C$ and δD measurements of CH_4 have been performed exclusively with mass spectrometry

(MS). Because of the very small mass difference (0.003 amu) between $^{13}CH_4$ and $^{12}CH_3D$, catalytic oxidation of CH_4 to CO_2 for $\delta^{13}C$ analysis and reduction of the resultant H_2O to H_2 for δD analysis must be carried out. High-resolution mass spectrometers ($\Delta M/M \sim 15000$) that could differentiate between $^{13}CH_4$ and $^{12}CH_3D$ are not available with the precision necessary for atmospheric research[23]; i.e., $\Delta\delta\ ^{13}C \approx 0.1–1‰$ and $\Delta\delta D \approx 1–10‰$. The conversion of CH_4 to CO_2 and H_2 requires the complete separation of the CH_4 from coexisting CO_2 and H_2O in the sample as well as from CO and higher hydrocarbons, which otherwise would also be converted to CO_2 and H_2O. In addition, N_2O has to be removed because of the mass interference between $^{12}C^{16}O_2$ and $^{14}N_2{}^{16}O$. Wahlen *et al.*[7] and Bösinger[24] describe sample preparation procedures in which preparative gas chromatography is used after the samples are purified with silica gel, a molecular sieve, or liquid nitrogen cold traps. Alternatively, Lowe and Brenninkmeijer[25] purify the samples using a series of liquid nitrogen cold traps and convert CO into CO_2 with I_2O_5 with subsequent removal of CO_2 at 77 K. The reported overall precisions are $\Delta\delta\ ^{13}C = \pm 0.05–0.2‰$[7,9,25] and $\Delta\delta D = \pm 2–3‰$.[16,26] The substantial effort required for sample processing has severely limited the quantity of available data on $\delta^{13}C$ and, in particular, on δD of atmospheric CH_4 and its sources.

We present here as a fundamentally different approach a direct measurement method for $\delta^{13}C$ and δD based on a tunable diode laser absorption spectrometer (TDLAS) in which we determine the $^{13}CH_4/^{12}CH_4$ and $^{12}CH_3D/^{12}CH_4$ ratios from the intensities of infrared absorption lines of the corresponding isotope pairs.

Webster and May[27] performed *in situ* measurements of stratospheric $^{13}CH_4/^{12}CH_4$ ratios with a balloonborne TDLAS instrument; however, the reported precision of $\Delta\delta^{13}C \sim \pm 90‰$ is insufficient to provide information on the atmospheric CH_4 cycle. There have been some previous efforts to apply TDLAS to measurements of naturally occurring isotope ratios in molecules other than CH_4. Measurements of $^{13}CO_2/^{12}CO_2$ ratios are described by Wong[28] with an accuracy of 3.1‰ (CO_2 concentration $\approx 5\%$) and by Becker *et al.*[29] with a precision of 4‰ (pure CO_2). Wahlen and Yoshinari[30] reported measurements of $N_2{}^{18}O/N_2{}^{16}O$ ratios on preconcentrated samples (precision 0.4‰). Lee and Majkowski[31] measured the $C^{18}O/C^{16}O$ and $C^{17}O/C^{16}O$ ratios in pure CO with a standard deviation of 2.5‰ for $C^{18}O/C^{16}O$. Using a TDLAS, Anderson *et al.* have performed laboratory studies of ozone isotopomers.[32]

We present here what is to our knowledge the first application of a TDLAS for stable isotope ratio measurements in CH_4, carried out directly on environmental samples collected in the field. Our earlier study on the development of the $\delta^{13}C$ technique has been communicated previously.[33] The further developments reported here include the extension of the method to δD measurements, the incorporation of a multipass reflection cell (White cell), which improves the CH_4-concentration limit by 2–3 orders of magnitude, modifications of the data evaluation procedure, and a more comprehensive study of possible spectroscopic interferences. In addition, an intercomparison of the TDLAS technique with conventional mass spectrometry has been performed for a variety of field samples from natural wetlands, landfills, and natural gas. The results demonstrate the applicability of our TDLAS instrument for $\delta\ ^{13}C$ and δD investigations of atmospheric CH_4 sources.

2. Experimental

A. Spectroscopy

The infrared absorption features of CH_4 in the middle and the near-infrared are determined by rotational–vibrational transitions of the CH_4 molecule. Although the main contribution of CH_4 to global warming comes from the ν_4 band at 1310 cm^{-1} in the atmospheric infrared window between 700 and 1400 cm^{-1}, the strongest absorption band of CH_4 is the ν_3 band at 3000 cm^{-1}. To investigate the applicability of this spectral region for isotope measurements, we recorded the spectra between 2800 and 3200 cm^{-1} at 0.02-cm^{-1} resolution for the different isotope species with a Fourier-transform infrared spectrometer (FTIR). The spectrum of CH_4 at natural isotopic abundance (i.e., containing 98.8% $^{12}CH_4$) and the spectra of pure $^{13}CH_4$ and pure $^{12}CH_3D$ are shown in Fig. 1. Because the symmetry of $^{12}CH_4$ and $^{13}CH_4$ is the same (spherical rotor), the pattern of absorption lines is similar for both isotopes, but the lines are shifted against each other by approximately 10 cm^{-1} because of the mass difference of the C atom. In contrast, $^{12}CH_3D$ is a symmetric top molecule with six fundamentals instead of four, and the additional quantum number K (orientation to the molecular axis) leads to a splitting of degenerate $^{12}CH_4$ states.

One approach for measurements of the $^{13}CH_4/^{12}CH_4$ ratio is to use the P or the R branch of $^{12}CH_4$ and $^{13}CH_4$, where some pairs of adjacent (< 0.5 cm^{-1}) and more or less sufficiently separated $^{13}CH_4$ and $^{12}CH_4$ lines or groups of lines exist. However, the typical intensity ratio of these lines is approximately the same as the natural isotope abundance ratio of $^{13}C/^{12}C$ (~ 0.01). Thus different optical pathways with the inverse length ratio would have to be used for these line pairs to achieve comparable absorptions for both isotope species.

Alternatively, the Q branch can be used for $^{13}CH_4/^{12}CH_4$ ratio measurements where some strong $^{13}CH_4$ lines neighbor weak $^{12}CH_4$ lines of similar line-center absorption. The region with the strongest $^{13}CH_4$ Q-branch lines is shown in Fig. 2; these spectra are recorded with the TDLAS instrument [(top) natural CH_4 and (bottom) $^{13}CH_4$]. Application of these line pairs does not require any compensation for the isotope abundance by different optical lengths. On the other hand, the weak $^{12}CH_4$ lines generally arise from rovibrational transitions with much higher ground-state energies than the $^{13}CH_4$ lines, resulting

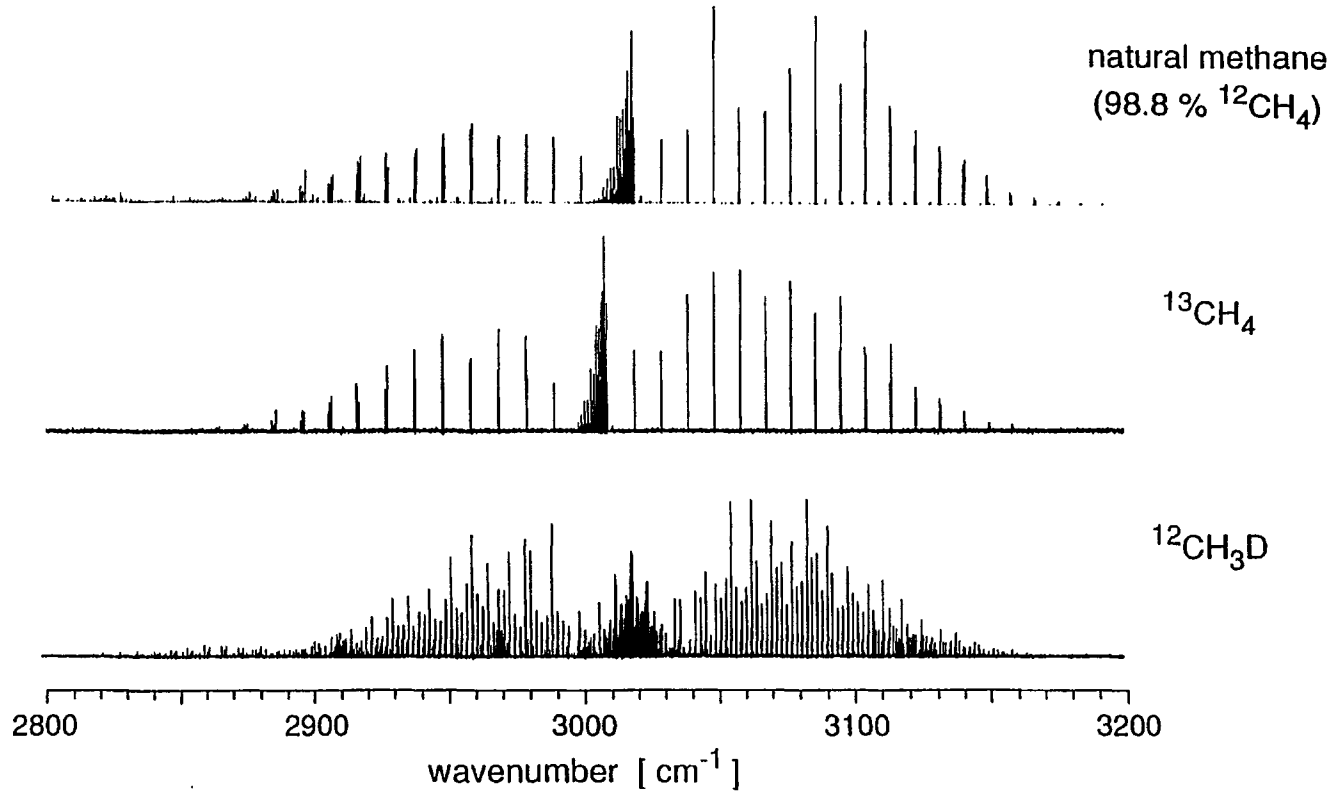

Fig. 1. FTIR spectra from 2800 to 3200 cm^{-1} (resolution 0.02 cm^{-1}). Top, CH_4 at natural isotopic composition (i.e., ~98.8% $^{12}CH_4$); middle, $^{13}CH_4$; bottom, $^{12}CH_3D$.

in a higher temperature dependence of the $\delta^{13}C$ measurements. This temperature dependence $\Delta\delta/\Delta T$ is proportional to the difference of ground-state energies (ΔE) of the corresponding transitions[34]:

$$\frac{\Delta\delta}{\Delta T} \approx \frac{\Delta E}{kT^2}\,1000(‰), \qquad (1)$$

where k is the Boltzmann constant and T is the absolute temperature. Measurements of the temperature coefficient $\Delta\delta^{13}C/\Delta T$ for the 3007.078-cm^{-1} ($^{12}CH_4$)/3007.145-cm^{-1} ($^{13}CH_4$) line pair yielded 22.2 ± 2.0‰/K,[33] in reasonable agreement with a value of 18‰/K calculated according to Eq. (1) for this line pair (ground-state energies, cf. Table 1, below). We show here that this relatively strong temperature dependence of the apparent $^{13}CH_4/^{12}CH_4$ isotope ratios measured with this line pair is adequately suppressed by the high thermal capacity of the gas cells and by procedures for zero measurements discussed below.

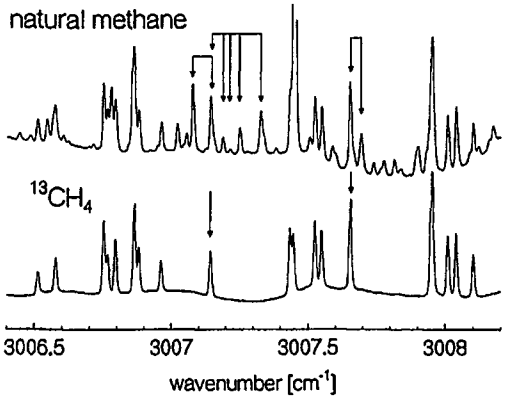

Fig. 2. TDLAS spectra. Top, natural CH_4 ($\delta^{13}C = -27.8‰$); bottom, pure $^{13}CH_4$. Possible $^{13}CH_4/^{12}CH_4$ line pairs are indicated by the arrows.

For measurements of the $^{12}CH_3D/^{12}CH_4$ ratio there is a higher number of suitable line pairs of comparable absorption spread over a much wider spectral range compared with the situation for the $\delta^{13}C$ measurements. Line pairs for $\delta^{13}C$ and δD measurements are discussed in detail below (Sections 3 and 4).

B. Optical Setup

The optical setup of the isotope TDLAS instrument is shown in Fig. 3. To facilitate the use of different lasers for the measurements of the $^{13}CH_4/^{12}CH_4$ ratio and the $^{12}CH_3D/^{12}CH_4$ ratio, we built a two-laser system. Two double-heterostructure Pb–salt diode lasers are mounted inside the same liquid nitrogen Dewar. Each laser can be independently temperature controlled in the range from 77 to 100 K. The divergent laser beam is collimated by an off-axis parabolic (OAP) mirror, and a plane mirror (PM1) can be switched manually to select the desired laser beam. Subsequently the laser beam passes through a Czerny–Turner-type monochromator to separate different longitudinal laser modes. A set of 12 CaF_2

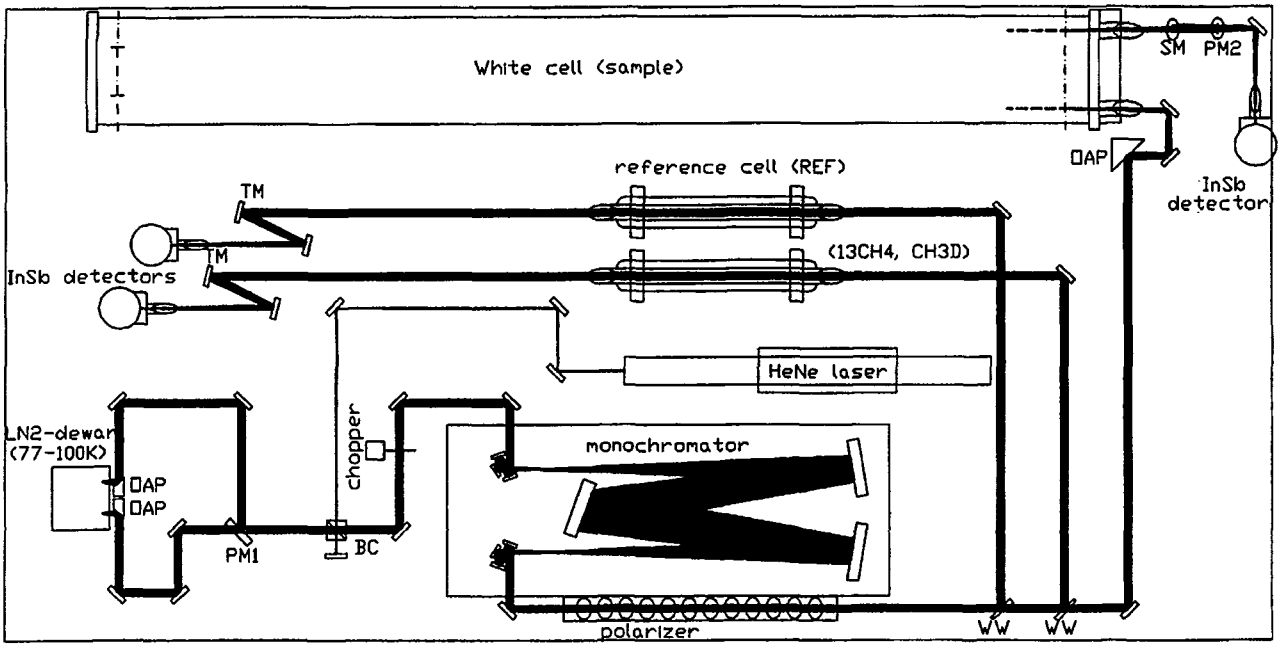

Fig. 3. Optical setup of the TDLAS instrument. See text for abbreviations.

Brewster plates linearly polarizes the laser beam to >99%. Two wedged CaF_2 windows (WW's) split the beam into three parts, with the main beam directed through a multipass reflection cell (White cell) that has a maximum optical length of 213 m (base length 1.50 m). At the entrance the beam is focused into the White cell with an OAP mirror. The outcoming beam from the White cell is directed by plane mirror PM2 up to the tilted spherical mirror (SM), which focuses the beam onto the detector. This arrangement compensates for the astigmatism of the White cell exit beam. The two reference beams formed by the beam splitters are directed through two 36-cm gas cells, one containing a CH_4-isotope reference gas and the other pure $^{13}CH_4$ or $^{12}CH_3D$. These beams are focused onto the InSb detectors with concave toroidal mirrors (TM's). To align the TDLAS instrument, one can coalign a He–Ne laser beam with the infrared beam, using a beam combiner (BC).

The windows of the gas cells and the detectors are mounted at the Brewster angle. Thus, in combination with the linear polarization of the laser beam, multiple beam interferences between the parallel surfaces of these optical elements are very effectively suppressed.[21,34,35] Interferences within the two beam splitters are prevented by their wedged shape.

C. Electronic Setup

Laser current control, data acquisition, processing, and analysis are performed by a digital signal processor card equipped with two 16-bit digital-to-analog converters and two 16-bit analog-to-digital converters mounted inside an 80286 PC. One digital-to-analog converter is used to generate a current ramp for tuning the laser wavelength over the absorption line pair of interest (scan time 300 ms). The second digital-to-analog converter permits the addition of a constant current within a single scan to jump over any spectral range between two absorption lines if necessary. This facilitates the combination[36] of all absorption line pairs within a given laser mode and the spectral transmission of the monochromator. Besides the two digital-to-analog-converter outputs, a 10-kHz sinusoidal modulation is added to the laser dc current. Demodulation of the detector outputs occurs by the use of lock-in amplifiers at the second harmonic (standard $2f$ lock-in technique[37]). In addition, the direct detector signals are passed through a low-pass filter to register the modulation-broadened direct absorption spectra. Thus, the progression of the laser power within a scan can be reconstructed, as discussed below. The three lock-in amplifier outputs and the three filtered direct signals are digitized by the two multiplexed analog-to-digital converters quasi-synchronously, with 1024 points per scan. Several spectra (typically 10) are coadded (i.e., $t = 10 \times 300$ ms) before processing.

D. Data Processing and Evaluation Procedure

The control of the experiment as well as the on-line evaluation of the spectra is performed with a C program operating on the digital signal processor. A host C program, which runs in parallel on the PC, controls graphic display, keyboard inputs through several menus, and data transfer between PC and digital signal processor card as well as additional functions such as the IEEE interface to the lock-in amplifiers.

Figure 4 shows an example set of simultaneously recorded and coadded (10×300 ms) $2f$ spectra used for measurements of the $^{13}CH_4/^{12}CH_4$ ratio. After each set of coadded scans the position of the $^{13}CH_4$

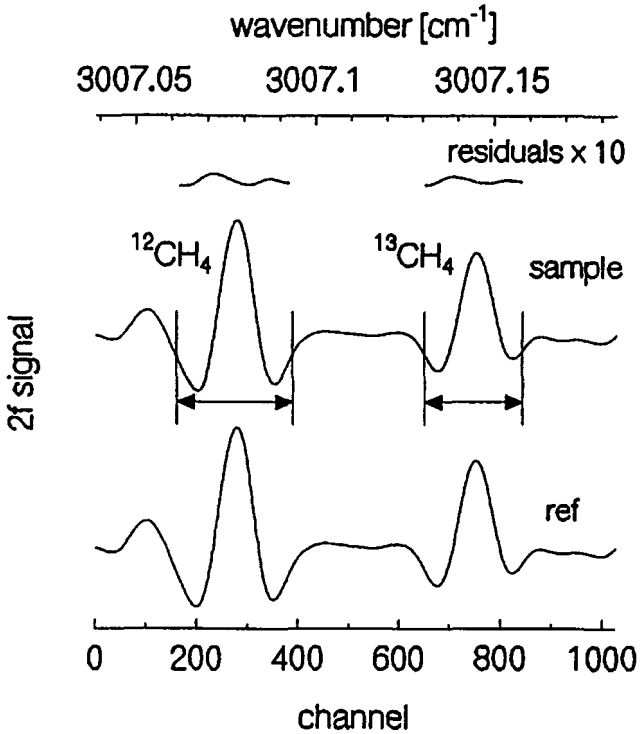

Fig. 4. δ ^{13}C measurement at the 3007.145-cm^{-1}/3007.078-cm^{-1} ($^{12}CH_4$) line pair: simultaneously recorded $2f$ spectra of (middle) a sample and (bottom) the reference gas (ref). The fits carried out according to Eqs. (2) and (3) are also shown in the sample spectrum, with the vertical lines marking the corresponding fit boundaries. However, at the scale used in the figure the fits cannot be distinguished from the recorded spectrum; the residuals of the fits are shown at the top (scale $\times 10$).

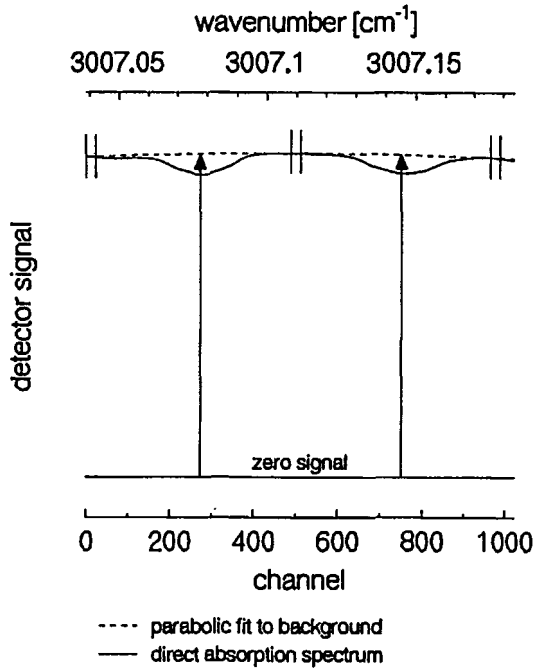

Fig. 5. Direct (modulation-broadened) absorption spectrum (sample), recorded simultaneously with the $2f$ spectra shown in Fig. 4. A parabolic fit is laid through three spectral intervals (marked by the vertical lines). The arrows indicate the derived total laser power at the ($2f$) line centers.

($^{12}CH_3D$) line is determined. The start voltage for the subsequent ramp is adjusted to compensate for drifts of the laser current and the temperature control units (line locking by laser current). In contrast to the δ evaluation procedure described previously,[33] here we use only the spectra of the sample and the isotope reference to determine the δ value of the sample. A multiple linear regression procedure is carried out on line for each set of spectra. One linear regression fits the $^{12}CH_4$ line of the reference gas to the $^{12}CH_4$ line of the sample:

$$\mathrm{spec}_{\mathrm{sample}}(i) = a_0\,\mathrm{spec}_{\mathrm{ref}}(i) + a_1 + a_2 i, \qquad (2)$$

where spec(i) is the ith point of the indicated spectrum and a_j are the regression coefficients. Analogously, the $2f$ absorption lines of $^{13}CH_4$ or $^{12}CH_3D$ are fitted to each other:

$$\mathrm{spec}_{\mathrm{sample}}(i) = b_0\,\mathrm{spec}_{\mathrm{ref}}(i) + b_1 + b_2 i. \qquad (3)$$

The δ value, relative to the reference gas, is obtained directly from the regression coefficients a_0 and b_0:

$$\delta = \left(\frac{b_0}{a_0}\gamma - 1\right)1000, \qquad (4)$$

where γ is a correction factor to compensate for the slightly different progression of the laser power within each scan at the different detectors. To reconstruct the variation of the total laser power within each scan we use the direct absorption spectra (Fig. 5) recorded simultaneously with the $2f$ spectra. Parabolic fits $p_{\mathrm{sample}}(i)$ and $p_{\mathrm{ref}}(i)$ are calculated with three intervals in nonabsorbing regions. The zero levels of the detector signals z_{sample} and z_{ref} are determined with a chopper, which is operated at the beginning of each measurement cycle. Thus the correction factor introduced in Eq. (4) can be calculated with

$$\gamma = \frac{(p_{\mathrm{sample}}(i_{16}) - z_{\mathrm{sample}})[p_{\mathrm{ref}}(i_{17}) - z_{\mathrm{ref}}]}{[p_{\mathrm{sample}}(i_{17}) - z_{\mathrm{sample}})[p_{\mathrm{ref}}(i_{16}) - z_{\mathrm{ref}}]}, \qquad (5)$$

where i_{16} and i_{17} signify the line-center position of the $^{12}CH_4$ and $^{13}CH_4$ (or $^{12}CH_3D$) absorption, as determined from the $2f$ spectra. Instead of the parabolic fit shown in Fig. 5, two linear fits can be calculated based on four spectral regions to the left and right of each absorption line. This procedure is preferred when a jump between the measurement lines is used. For each measurement cycle approximately 30 consecutive sets of spectra are analyzed according to the described procedure, and the δ values obtained from Eq. (4) are averaged.

E. Sample Handling and Automated Cell-Filling Procedure

The direct absorption line shapes and the corresponding measured $2f$ line shapes depend on the pressure, temperature, and fractional absorption of the gas.

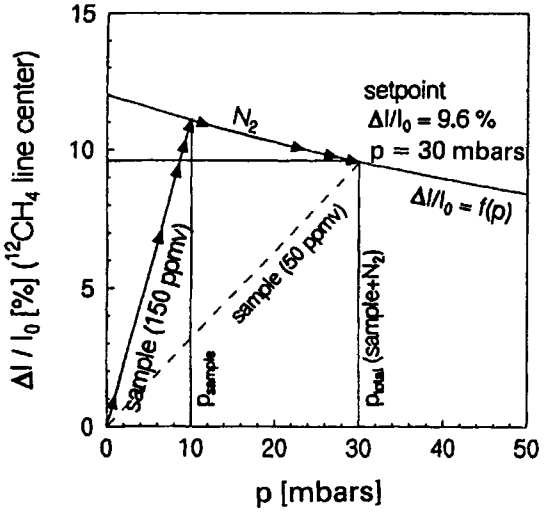

Fig. 6. Illustration of the automated White-cell-filling procedure.

In the pressure region near 30–50 mbars the absorption line shape is a Voigt profile, i.e., a convolution of a Lorentzian profile (pressure broadening) and a Gaussian profile (Doppler broadening). At fractional absorptions ($\Delta I/I_0$) of several percent the deviation between the observed absorption line shape and the optical density (od) has to be taken into account:

$$\frac{\Delta I}{I_0} = 1 - \exp(-\mathrm{od}) = \mathrm{od} - \frac{1}{2}\mathrm{od}^2 + \frac{1}{6}\mathrm{od}^3 - + \ldots . \tag{6}$$

Measurements of the apparent $\delta\,^{13}C$ dependence on mismatches in pressure and fractional absorption between the sample cell and the reference cell for TDLAS measurements were discussed previously.[33] (For the 3007.078-cm^{-1} ($^{12}CH_4$)/ 3007.145-cm^{-1} ($^{13}CH_4$) line pair, a pressure dependence of $\Delta\delta^{13}C/\Delta p$ = 5.2 ± 0.4‰/mbars and a fractional absorption dependence of $\Delta\delta^{13}C/\Delta(\Delta I/I_0)$ = 1.0 ± 0.3‰/percent fractional absorption were measured.

To ensure good matching of the total pressure and fractional absorption between the sample and the reference cell, we have devised an automatic filling procedure that uses computer-controlled magnetic valves. In a first step the sample inlet valve is opened to the evacuated White cell for a defined, brief period of time, and the resulting increase in $^{12}CH_4$ absorption is measured. Using the relationship between opening time of the sample valve and increase of absorption determined in this manner, one can introduce the sample stepwise into the White cell until the required absorption is reached. Afterward, N_2 is added in a similar stepwise manner with the measured relationship between N_2 valve opening time and pressure increase. For a given CH_4 amount inside the White cell the line-center absorption decreases with increasing total pressure (owing to pressure broadening; see Fig. 6). Therefore the set point of the desired final line-center absorption has to be corrected during the CH_4-sample-filling procedure depending on the mixing ratio of CH_4 in the sample gas. This procedure ensures that the absorption is correct after the N_2 is added up to the desired total pressure.

While the gases are being added to the White cell, they are continuously pumped around a closed circuit to ensure thorough mixing. The gas circuit also contains a liquid nitrogen cold trap to remove water from the sample. The precision of the system's ability to adjust the fractional absorption is $\Delta(\Delta I/I_0)$ = ±0.001–0.002, and the reproducibility of the total pressure adjustment is Δp = ±0.02 mbars. The CH_4 mixing ratio m of the sample can be determined from the measurement of $\Delta I/I_0$ at the $^{12}CH_4$ line center, the pressure of the sample gas alone ($p_{\mathrm{sample,WC}}$), and the pressure after adding the N_2 ($p_{\mathrm{total,WC}}$):

$$m = m_{\mathrm{ref}} \frac{l_{\mathrm{ref}}}{l_{\mathrm{WC}}} \frac{p_{\mathrm{total,WC}}}{p_{\mathrm{sample,WC}}} \frac{p_{\mathrm{total,ref}}}{p_{\mathrm{total,WC}}} \frac{\ln[1 - (\Delta I/I_0)_{\mathrm{WC}}]}{\ln[1 - (\Delta I/I_0)_{\mathrm{ref}}]} \beta, \tag{7}$$

where l_{ref} and l_{WC} are the optical lengths of the reference and the White cell, respectively; m_{ref} is the mixing ratio of the reference gas in the reference cell; and β is a calibration factor, determined with a (mixing-ratio) calibration gas containing 1000 parts in 10^6 by volume (ppmv) CH_4.

F. Calibration versus the PDB/SMOW Scale

Alternating with the sample measurements, the reference gas is introduced into the White cell with the above automated procedure and measured against itself. The mean of two such $\delta_{\mathrm{TDLAS}}^{\mathrm{ref}}$(ref) (Ref. 38) zero measurements is subtracted from the measured $\delta_{\mathrm{TDLAS}}^{\mathrm{ref}}$(sample) value of the sample. This compensates for slow (>30 min) drifts, which mainly arise from small changes in the temperature difference between the White cell and the reference cell and from slight changes in the optical beam alignment as a result of thermal effects and of the pressure cycling within the White cell.

These measurements yield the relative deviation of the $^{13}CH_4/^{12}CH_4$ or $^{12}CH_3D/^{12}CH_4$ ratio of the sample against the reference gas. The isotope ratios of the reference gas on the PDB/SMOW scales have been determined with MS to be $\delta^{13}C_{\mathrm{MS}}^{\mathrm{PDB}}$(ref) = −27.79 ± 0.04‰ (mean ± 1σ, n = 3) and $\delta D_{\mathrm{MS}}^{\mathrm{SMOW}}$(ref) = −164.9 ± 2.8‰ ($n$ = 2). To ensure the correct coupling of the $\delta^{13}C_{\mathrm{TDLAS}}^{\mathrm{ref}}$(sample) and the $\delta D_{\mathrm{TDLAS}}^{\mathrm{ref}}$(sample) measurements to the PDB/SMOW scales, calibration gases of isotopic compositions clearly distinct from the reference gas are measured. Because standard gases of known $^{13}CH_4/^{12}CH_4$ and $^{12}CH_3D/^{12}CH_4$ isotopic composition are not available, we produced our own mixtures of the reference gas and pure $^{13}CH_4$ or $^{12}CH_3D$. Mass spectrometer analysis of our currently used $\delta^{13}C$ calibration gas(cal) yielded $\delta^{13}C_{\mathrm{MS}}^{\mathrm{PDB}}$(cal) = 9.17 ± 0.06‰ ($n$ = 3) and $\delta D_{\mathrm{MS}}^{\mathrm{SMOW}}$(cal) = 25.9 ± 0.1‰ ($n$ = 2) for the δD calibration gas. The TDLAS measurements of these calibration gases [$\delta_{\mathrm{TDLAS}}^{\mathrm{ref}}$(cal)] yield a transformation

factor α:

$$\alpha = \frac{\delta_{MS}^{PDB/SMOW}(cal) - \delta_{MS}^{PDB/SMOW}(ref)}{\delta_{TDLAS}^{ref}(cal)\left[1 + \frac{\delta_{MS}^{PDB/SMOW}(ref)}{1000}\right]}. \quad (8)$$

The need for such a transformation factor is discussed in Subsections 3.A.2. and 4.A.2, below, and arises from the presence of weak underlying absorptions from other CH_4 isotopomers for some line pairs. For each measurement series at least three TDLAS measurements of the corresponding calibration gas are carried out to yield an average value of α, as determined from Eq. (8). With the mean α, the TDLAS δ results for the samples $[\delta_{TDLAS}^{ref}(sample)]$ can be converted to the PDB/SMOW values according to

$$\delta_{TDLAS}^{PDB/SMOW}(sample) = \delta_{MS}^{PDB/SMOW}(ref) + \alpha\left[1 + \frac{\delta_{MS}^{PDB/SMOW}(ref)}{1000}\right] \times \delta_{TDLAS}^{ref}(sample). \quad (9)$$

3. $\delta^{13}C$ Measurements

A. Line-Pair Selection Criteria

1. *General Considerations*

In the spectral region between 2800 and 3200 cm^{-1}, $^{12}CH_4/^{13}CH_4$ line pairs of comparable absorption are found mainly between 3000 and 3010 cm^{-1}. Table 1 presents an overview of suitable line pairs, based on the HITRAN 92 data.[39] Because the variation of the laser power between the different absorption lines (as discussed above) increases with the spectral separation of the lines, this separation should be much lower (<0.1 cm^{-1}) than the tuning range of the laser modes and the spectral resolution of the monochromator (0.5–1 cm^{-1}). On the other hand, at $T \sim 300$ K and at low pressures (30–50 mbars), where the width of the absorption lines is dominated by Doppler broadening, the spectral separation has to be $> \sim 0.04$ cm^{-1} for sufficient resolution of the two lines. In addition, the line strengths of the selected line pairs should be as high as possible to minimize the necessary CH_4 mixing ratios. On the basis of these criteria, the $^{13}CH_4$ lines at 3007.145 and at 3007.653 cm^{-1} seem to be the best candidates. The $^{13}CH_4$ line at 3007.145 cm^{-1} may be combined either with the $^{12}CH_4$ line at 3007.188 cm^{-1} or with the $^{12}CH_4$ line at 3007.078 cm^{-1}. Although the difference in ground-state energies for the 3007.145-cm^{-1}/3007.188-cm^{-1} line pair is approximately a factor of 15 lower than for the 3007.145-cm^{-1}/3007.078-cm^{-1} line pair, we measured the effective temperature dependence for the first line pair to be only a factor of approximately 2 lower. This is due to the existence of underlying $^{12}CH_4$ absorption lines, which are discussed below. The absorption of the 3007.078-cm^{-1} $^{12}CH_4$ line is, however, approximately 3 times stronger than the absorption of the 3007.188-cm^{-1} $^{12}CH_4$ line and roughly equal to the absorption of the 3007.145-cm^{-1} $^{13}CH_4$ line, resulting in a lower CH_4 mixing ratio limit and a lower $\Delta\delta^{13}C/\Delta(\Delta I/I_0)$ dependence. Therefore, for the $\delta^{13}C$ measurements presented here, we used the 3007.145-cm^{-1}/3007.078-cm^{-1} line pair. To judge the wisdom of the choice of this (or an alternative) line pair, one has to investigate several items concerning their spectroscopic properties, as shown below.

2. *Possible Interdependence of the Two Absorption Lines*

Whereas the 3007.078-cm^{-1} $^{12}CH_4$ line is free of $^{13}CH_4$ absorptions, there are some $^{12}CH_4$ absorption features underlying the $^{13}CH_4$ line at 3007.145 cm^{-1}, which can be recognized by the weak shoulders on the wings of this line in the spectrum of natural methane (Fig. 2; compare this line shape with that in the $^{13}CH_4$ spectrum). The HITRAN 92 database lists two $^{12}CH_4$ lines at 3007.143 and 3007.145 cm^{-1} (see Table 1). It should be noted, however, that the HITRAN data given in Table 1 are derived from spectra with resolutions of 0.01–0.02 cm^{-1}, and thus they often combine different lines separated by less than 0.02 cm^{-1} into a single line position and partition the total line strength equally.[40] Even though the underlying $^{12}CH_4$ absorption lines are not at exactly the same position as the $^{13}CH_4$ line at 3007.145 cm^{-1}, their influence can be compensated for with sufficient accuracy by the calibration procedure described above. The transformation factor α, determined according to Eq. (8) for this line pair, was measured to be $\alpha = 1.28 \pm 0.02$ ($n = 17$), suggesting that the absorption of the underlying $^{12}CH_4$ features are approximately 30% of the absorption of the $^{13}CH_4$ line. Measurements of α for the 3000.734-cm^{-1}/3001.194-cm^{-1} line pair yielded values of $\alpha = 1.00 \pm 0.03$ ($n = 5$), indicating that this is a pair of unblended (but weaker) $^{12}CH_4$ and $^{13}CH_4$ lines.

3. *Interferences from Underlying $^{12}CH_3D$ Absorptions*

Underlying $^{12}CH_3D$ absorptions could cause the δD value of the sample to influence the $\delta^{13}C$ measurement. We detected a weak $^{12}CH_3D$ absorption at 3007.097 cm^{-1}, which is not in the HITRAN 92 database. This $^{12}CH_3D$ line is sufficiently separated from the $^{12}CH_4$ line at 3007.078 cm^{-1} to have a negligible effect on the $\delta^{13}C$ measurements. Even if their line positions were the same, the maximum contribution of the $^{12}CH_3D$ line [$S \approx 4 \times 10^{-24}$ $cm^{-1}/(mol\ cm^{-2})$] would result in an error of $\Delta\delta^{13}C = \pm 0.5‰$, assuming a maximum range in δD of $\pm 150‰$.

4. *Interferences from Gases Other than CH_4*

A weak absorption line from H_2O [$S = 1.0 \times 10^{-25}$ $cm^{-1}/(mol\ cm^{-2})$] exists at 3007.128 cm^{-1} and is separated by 0.017 cm^{-1} from the $^{13}CH_4$ line at 3007.145 cm^{-1}. The procedure for drying the samples described above ensures that the effect of

Table 1. $^{13}CH_4$ Line Pairs of Comparable Intensities (from HITRAN 92[a])

Position		Transition		S	E_{ground}	
$^{13}CH_4$	$^{12}CH_4$	Band	Quantum Numbers[c]	[cm^{-1}/(mol cm^{-2})]	(cm^{-1})	Interferences[b]
3000.734		ν_3	12, E, 1	1.0×10^{-22}	814.7	
3000.734		ν_3	12, $F1$, 1	1.0×10^{-22}	814.7	
3000.734		ν_3	12, $A1$, 1	1.0×10^{-22}	814.7	
	3001.194	ν_3	18, $F2$, 1	1.2×10^{-22}	1778.2	O_3, CH_3Cl
	3001.194	ν_3	18, $A2$, 1	2.1×10^{-22}	1778.2	H_2O (3001.175, $S = 3.3 \times 10^{-25}$)
	3001.194	ν_3	18, E, 1	8.4×10^{-23}	1778.2	
3003.094		ν_3	10, E, 1	2.7×10^{-22}	575.1	
3003.099		ν_3	10, $F2$, 1	2.7×10^{-22}	575.1	
3003.101		ν_3	10, $A2$, 1	2.7×10^{-22}	575.1	
	3002.853	ν_3	17, $F2$, 1	6.3×10^{-22}	1592.4	O_3, CH_3Cl
3006.097		ν_3	8, $F2$, 1	2.8×10^{-22}	376.8	
		ν_3	12, $F1$, 3			$^{12}CH_4$ (3006.072, $S = 6.3 \times 10^{-23}$)
		$\nu_3 + \nu_4 - \nu_3$	10, $A2$, 1			$^{12}CH_4$ (3006.097, $S = 2.6 \times 10^{-22}$)
		ν_3	12, $F2$, 3			$^{12}CH_4$ (3006.108, $S = 5.9 \times 10^{-23}$)
	3006.155	ν_3	12, $A2$, 1	2.1×10^{-22}	815.1	O_3, CH_3Cl
3007.145		ν_3	7, $F1$, 2	4.5×10^{-22}	293.2	
		$2\nu_2$	6, $A2$, 1			$^{12}CH_4$ (3007.143, $S = 2.3 \times 10^{-22}$)
		$\nu_3 + \nu_4 - \nu_4$	8, $A2$, 1			$^{12}CH_4$ (3007.145, $S = 4.5 \times 10^{-22}$)
	3007.078	ν_3	16, $F2$, 1	5.5×10^{-22}	1417.1	O_3, CH_3Cl
	3007.078	ν_3	16, $F1$, 2	5.5×10^{-22}	1417.1	H_2O (3007.128, $S = 1.0 \times 10^{-25}$)
						$^{12}CH_3D$ (3007.097, $S = 4 \times 10^{-24}$)[d]
	3007.188	$2\nu_2$	6, $F2$, 2	2.9×10^{-22}	219.9	O_3, CH_3Cl
	3007.210	$2\nu_2$	6, $F2$, 1	9.0×10^{-23}	219.9	H_2O (3007.128, $S = 1.0 \times 10^{-25}$)
	3007.250	$2\nu_2$	6, $F1$, 1	4.6×10^{-22}	219.9	H_2O (3007.210, $S = 2.6 \times 10^{-26}$)
	3007.328	$2\nu_2$	6, $A1$, 1	7.2×10^{-22}	219.9	H_2O (3007.210, $S = 2.6 \times 10^{-26}$)
	3007.328	$\nu_3 + \nu_4 - \nu_4$	9, $F1$, 1	7.9×10^{-23}	1728.6	H_2O (3007.301, $S = 6.3 \times 10^{-26}$)
	3007.328	$\nu_3 + \nu_4 - \nu_4$	6, $F1$, 1	7.9×10^{-23}	1558.5	
	3007.328	$\nu_3 + \nu_4 - \nu_4$	8, $F1$, 1	7.9×10^{-23}	1679.6	
	3007.328	$\nu_3 + \nu_4 - \nu_4$	8, $F2$, 1	7.9×10^{-23}	1641.2	
3007.653		ν_3	6, $A1$, 1	5.2×10^{-22}	219.9	
		$\nu_3 + \nu_4 - \nu_4$	7, E, 1			$^{12}CH_4$ (3007.653, $S = 5.2 \times 10^{-22}$)
		$\nu_3 + \nu_4 - \nu_4$	8, E, 1			$^{12}CH_4$ (3007.653, $S = 5.2 \times 10^{-22}$)
		ν_3	11, $F1$, 2			$^{12}CH_4$ (3007.670, $S = 2.4 \times 10^{-22}$)
	3007.692	$\nu_3 + \nu_4 - \nu_4$	7, $F1$, 1	1.2×10^{-22}	1562.8	O_3, CH_3Cl
	3007.692	$\nu_3 + \nu_4 - \nu_4$	7, $F1$, 2	1.2×10^{-22}	1597.6	
	3007.692	$\nu_3 + \nu_4 - \nu_4$	8, $F2$, 2	1.2×10^{-22}	1639.5	
	3007.693	ν_3	18, $F2$, 5	1.1×10^{-22}	1780.7	
	3007.693	ν_3	17, $A2$, 1	4.5×10^{-22}	1593.8	

[a]Ref. 39.
[b]Listed if separated by less than 0.030 cm^{-1} from either the $^{12}CH_4$ or the $^{13}CH_4$ measurement lines; underlying $^{12}CH_4$ absorptions are listed only if their line strengths are higher than 10% of the total line strength of the $^{13}CH_4$ line(s).
[c]J, C, N (ground state).
[d]Not listed in HITRAN 92; the position and line strength of this $^{12}CH_3D$ line have been calculated from TDLAS and FTIR spectra.

this H_2O absorption is negligible. Several absorptions of O_3 and CH_3Cl are listed in HITRAN 92 for the region near the 3007.145-cm^{-1}/3007.078-cm^{-1} $^{13}CH_4/^{12}CH_4$ line pair and near all other line pairs listed in Table 1. However, their contributions are negligible as well. Although there is no evidence from the HITRAN 92 data about possible interferences from nonmethane hydrocarbons (NMHC's), they might interfere in the given spectral region, because the C–H bond-stretching vibration frequencies are around 3000 cm^{-1}. For two natural gas samples a weak interference near the 3000.734-cm^{-1}/3001.194-cm^{-1} line pair was observed, probably because of ethane, propane, or further NMHC's present in these samples. For the 3007.145-cm^{-1}/3007.078-cm^{-1} line pair, however, no interfering absorptions were observed for these samples. We have not yet carried out a comprehensive study of the spectra of the most abundant NMHC's, but the good agreement of $\delta^{13}C_{TDLAS}$ and $\delta^{13}C_{MS}$ values for unpurified samples from various CH_4 sources including landfills (see below) strongly suggests that neither NMHC's nor other species interfere with the $\delta^{13}C$ measurements at the 3007.145-cm^{-1}/3007.078-cm^{-1} line pair for these samples.

B. Reproducibility

The reproducibility achieved for the $\delta^{13}C$ measurements is ±0.5‰. With the given pressure and absorption dependences (see above), the uncertainty in

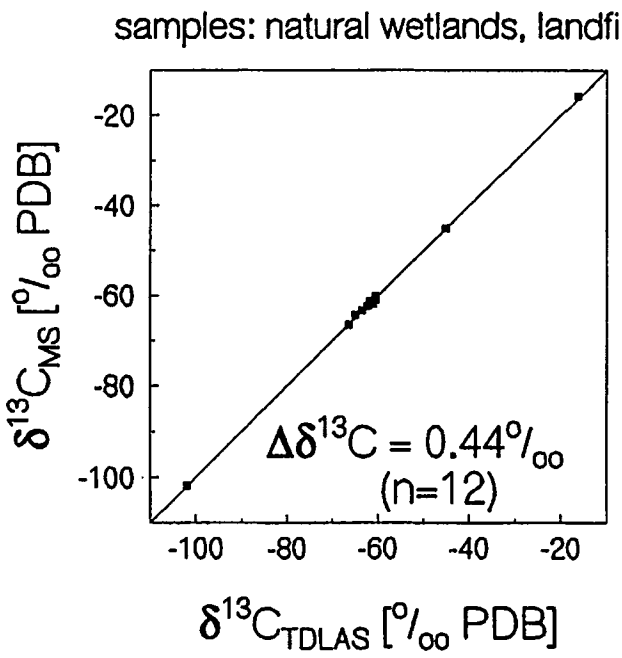

Fig. 7. Intercomparison between TDLAS and MS; $\delta^{13}C$ measurements for various samples from natural wetlands and landfills. The mean deviation is $\Delta\delta^{13}C = 0.44‰$.

adjustment of these two parameters with the automatic sample-filling system may contribute at most $\Delta\delta^{13}C \approx 0.1$–$0.2‰$ ($\Delta I/I_0$) and $\Delta\delta\ ^{13}C \approx 0.1‰$ (pressure). The $\delta\ ^{13}C$ reproducibility is probably dominated by drifts (insofar as they are not compensated by the zero measurements) in the temperature difference between the cells and in beam alignment. Currently the mixing-ratio limit for direct measurements (i.e., without any preconcentration of the CH_4 in environmental samples) is >50 ppmv, corresponding to 2 μmol CH_4 in the 28-l White cell.

C. Comparison TDLAS versus MS

An intercomparison between our TDLAS instrument and the mass spectrometer technique has been performed for various samples from natural wetlands and landfills. For the wetland samples, CH_4 release was encouraged by physical perturbation of the sediments. The landfill samples include several samples from gas wells, a surface emission sample collected with a static chamber, and a soil gas sample taken from a landfill cover. The CH_4 concentrations ranged from 1700 ppmv to 80 vol. %. The samples were stored in gas-tight sampling bags made of polyethylene-coated weldable aluminium foil. For TDLAS analysis no sample preparation was necessary. The preparation of samples for mass spectrometer $\delta^{13}C$ analysis was performed at the Institut für Umweltphysik, Universität Heidelberg, as described by Levin *et al.*[20] Figure 7 shows the results of the intercomparison. The mean deviation[41] in $\delta^{13}C$ between TDLAS and MS is $\Delta\delta^{13}C = 0.44‰$, where some TDLAS values are averages of more than one measurement. Comparing only single TDLAS measurements with the MS values yields a mean deviation of $\Delta\delta^{13}C = 0.59‰$. This result demonstrates the applicability of the TDLAS instrument for $\delta^{13}C$ measurements of atmospheric CH_4 sources, for which the $\delta^{13}C$ variations are typically markedly larger than the achieved accuracy.

4. δD Measurements

A. Line Selection

1. *General Considerations*

In contrast to the situation for $^{13}CH_4/^{12}CH_4$, there are many $^{12}CH_3D/^{12}CH_4$ line pairs of comparable absorption spread over the spectral region between ~ 2900 and ~ 3150 cm^{-1}. Some of the possible candidate pairs are listed in Table 2; lines with significant interferences from H_2O ($S > 10^{-24}$ cm^{-1}/(mol cm^{-2})) have been excluded. We normally used either the 3042.345-cm^{-1} ($^{12}CH_3D$)/3042.221-cm^{-1} ($^{12}CH_4$) line pair or the line pair at 3044.289 cm^{-1} ($^{12}CH_3D$)/3044.170 cm^{-1} ($^{12}CH_4$) (standard line pairs). There are also some strong $^{12}CH_3D$ lines above 3050 cm^{-1} (cf. Fig. 1); however, our present diode lasers only cover the spectral region up to approximately 3050 cm^{-1}. As examples, two possible line pairs above 3050 cm^{-1} are listed in Table 2 (based on HITRAN 92 data).

Generally, for δD measurements the temperature, pressure, and absorption dependences are of lesser importance than they are for the $\delta^{13}C$ measurements, as the required precision is lower. On the other hand, δD measurements are more sensitive to spectroscopic interferences, because the $^{12}CH_3D$ lines are approximately a factor of 20 weaker than the $^{13}CH_4$ lines. A discussion of the $^{12}CH_3D/^{12}CH_4$ line pairs follows that is similar to the discussion presented above for the $^{13}CH_4/^{12}CH_4$ line pairs.

2. *Possible Interdependence of the Two Absorption Lines*

We determined transformation factors $\alpha = 1.03 \pm 0.03$ ($n = 10$) for the 3042.345-cm^{-1}/3042.221-cm^{-1} line pair and $\alpha = 1.00 \pm 0.02$ ($n = 4$) for the 3044.289-cm^{-1}/3044.170-cm^{-1} line pair. This result indicates pairs of pure ($> \sim 97\%$) absorptions of $^{12}CH_3D$ and $^{12}CH_4$, respectively.

3. *Interferences from Underlying $^{13}CH_4$ Absorptions*

In the HITRAN 92 database there is no indication of $^{13}CH_4$ interferences within the spectral regions of the two standard $^{12}CH_3D/^{12}CH_4$ line pairs (cf. Table 2). Thus δD measurements should be independent of $\delta^{13}C$ values of the samples.

4. *Interferences from Gases Other than CH_4*

Some weak H_2O absorptions lie in the spectral region of the 3042.345-cm^{-1}/3042.221-cm^{-1} line pair (cf. Table 2). The drying procedure is sufficient to suppress the effect of these H_2O lines. For the 3044.289-cm^{-1}/3044.170-cm^{-1} line pair no H_2O absorptions are known. For these two line pairs, as well as for

Table 2. $^{12}CH_3D/^{12}CH_4$ Line Pairs (from HITRAN 92)

Position		Transition		S	E_{ground}	
$^{12}CH_3D$	$^{12}CH_4$	Band	Quantum Numbers[a]	[$cm^{-1}/(mol\ cm^{-2})$]	(cm^{-1})	Interferences
2950.851		ν_4	7, 6	2.8×10^{-23}	266.3	
	2951.306	$\nu_2 + \nu_4$	10, *F*1, 2	1.2×10^{-22}	575.3	O_3, CH_3Cl
2970.370		ν_4	6, 0	1.6×10^{-23}	162.9	
2970.409		ν_1	10, 7	1.6×10^{-23}	492.9	
	2970.335	$2\nu_2$	11, *E*, 1	1.7×10^{-23}	689.9	O_3
	2970.309	$2\nu_2$	11, *F*2, 2	3.2×10^{-23}	689.9	H_2O (2970.403, $S = 5.0 \times 10^{-26}$)
	2970.261	$2\nu_2$	11, *A*2, 1	4.5×10^{-23}	689.9	H_2O (2970.404, $S = 2.1 \times 10^{-27}$)
3042.345		ν_1	8, 4	7.3×10^{-24}	300.9	
3042.345		ν_4	2, 1	7.3×10^{-24}	24.6	
	3042.221	ν_1	11, *F*2, 1	1.6×10^{-23}	689.7	O_3, CH_3Cl
						H_2O (3042.328, $S = 1.5 \times 10^{-25}$)
						H_2O (3042.368, $S = 1.3 \times 10^{-25}$)
3044.289[b]		ν_4	2, 2	2.0×10^{-23}	28.8	
	3044.170	$\nu_2 + \nu_4$	12, *E*, 2	7.9×10^{-23}	815.0	O_3, CH_3Cl
3061.414		ν_4	4, 3	4.4×10^{-23}	89.9	
	3061.493	$\nu_3 + \nu_4 - \nu_4$	4, *F*2, 1	9.8×10^{-23}	1434.6	O_3, CH_3Cl
3068.950		ν_4	5, 3	3.7×10^{-23}	128.7	
	3068.573	$2\nu_2$	4, *F*1, 1	5.8×10^{-23}	104.8	O_3, CH_3Cl
						H_2O (3068.932, $S = 3.1 \times 10^{-25}$)

[a] J, K for $^{12}CH_3D$ and J, C, N for $^{12}CH_4$ ground (state).
[b] From HITRAN 86 (Ref. 42).

most of the other candidates, interferences with O_3 and CH_3Cl are listed in the HITRAN 92 database but are not significant for the δD measurements. For two natural gas samples an interfering absorption near the 3042.345-cm^{-1} $^{12}CH_3D$ line was observed (attributed to ethane, propane, or further NMHC's present in the natural gas); however, the line positions were such that no influence on the measurements was apparent. The comparison with the MS measurements further confirms that interferences do not disturb the δD measurements.

B. Reproducibility

The reproducibility for δD measurements (the same line pair is used) is ~ ±2‰. The lower mixing-ratio limit for direct δD measurements is ~2000 ppmv CH_4, which corresponds to 80 μmol CH_4 in our White cell.

C. Comparison of TDLAS versus MS and Comparison of TDLAS Measurements with Two Different Line Pairs

To conduct the comparison between TDLAS and MS, we used landfill samples from gas wells (n = 3) and natural gas samples (n = 2). The CH_4 concentrations in the samples ranged between 6.3% and ~99%. MS measurements of δD were performed at the Bundesanstalt für Geowissenschaften und Rohstoffe, Hannover, Germany.[26] The mean deviation[41] between TDLAS and MS is ΔδD = 5.1‰ (n = 5) (Fig. 8); TDLAS (and MS) analyses were performed only once for each sample. This mean deviation is not distinctly larger than the reproducibility of the MS δD values of ~ ±3‰ and clearly demonstrates the capability of the TDLAS instrument for high-precision δD measurements.

Beside possible systematic errors concerning the calibration procedure (see below) the main systematic

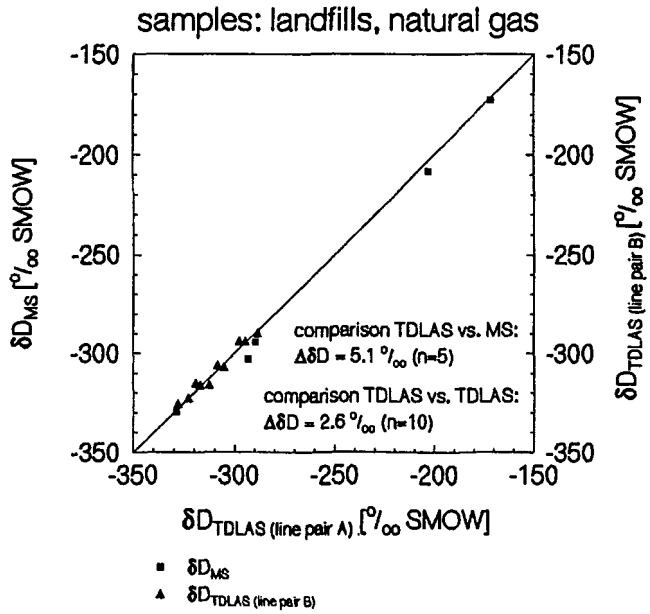

Fig. 8. Intercomparison between TDLAS and MS δD measurements for various landfill and natural gas samples (n = 5); the mean deviation is ΔδD = 5.1‰. In addition, the intercomparison between TDLAS measurements with the two different standard $^{12}CH_3D/^{12}CH_4$ line pairs is shown; the mean deviation is ΔδD = 2.6‰. A is the line pair at 3042.345 cm^{-1}/3042.221 cm^{-1}, and B is the line pair at 3044.289 cm^{-1}/3044.170 cm^{-1}.

Table 3. Two Examples of $^{13}CH_4/^{12}CH_4$ Line Pairs from the *R* Branch[a] (from HITRAN 92[b])

Position		Transition		S	E_{ground}	
$^{13}CH_4$	$^{12}CH_4$	Band	Quantum Numbers[c]	[$cm^{-1}/(mol\ cm^{-2})$]	(cm^{-1})	Interferences
3028.852		ν_3	1, *F*1, 1	9.5×10^{-22}	10.5	
	3028.752	ν_3	0, *A*1, 1	9.5×10^{-20}	0.0	O_3, CH_3Cl
						H_2O (3028.764; $S = 6.0 \times 10^{-27}$)
						H_2O (3028.877; $S = 1.3 \times 10^{-25}$)
3038.613		ν_3	2, *E*, 1	1.2×10^{-21}	31.4	
3038.629		ν_3	2, *F*2, 1	8.3×10^{-22}	31.4	
	3038.499	ν_3	1, *F*1, 1	8.9×10^{-20}	10.5	O_3, CH_3Cl

[a]The ratio of line strengths is about equal to the ratio of abundance of the two isotopomers (~1:100).
[b]Ref. 39.
[c]*J*, *C*, *N* (ground state).

error that might cause the overall δD (as well as the $\delta^{13}C$) accuracy to be poorer than the reproducibility could arise from spectroscopic interferences from unknown gases in the sample (see Subsection 4.A.4). This potential error can be excluded by subsequent measurements with different line pairs. We carried out this comparison for the two standard $^{12}CH_3D/^{12}CH_4$ line pairs for various landfill samples (Fig. 8). The mean deviation for this internal TDLAS intercomparison is $\Delta\delta D = 2.6‰$ ($n = 10$), supporting the quality of the δD measurements.

The fact that the intercomparison between TDLAS and MS δD measurements is slightly poorer than the intercomparison between the two standard line pairs might be the result of a slight nonlinearity in the TDLAS calibration. At present the δD calibration is fixed at the two points $\delta D = -164.9‰$ and $\delta D = 25.9‰$ of the SMOW scale, thus the typical range of δD for atmospheric methane sources is not fully covered. This also applies to the $\delta^{13}C$ calibration, which is fixed at $\delta^{13}C = -27.79‰$ and $\delta^{13}C = 9.17‰$ PDB. There is a general need for adequate δD and $\delta^{13}CCH_4$ standard gases for both the TDLAS calibration and the MS measurements (which usually use H_2O standards for δD calibration and CO_2 standards for $\delta^{13}C$ calibration).

5. Discussion

In contrast to the situation for δD measurements, $^{13}CH_4/^{12}CH_4$ line pairs of comparable intensity are much scarcer. The line pair used in this study at 3007.145 cm^{-1}/3007.078 cm^{-1} is adequate for CH_4-source measurements despite having some disadvantages such as the impurity of the $^{13}CH_4$ line and, more important, the strong temperature dependence of the intensity ratio. For the $\delta^{13}C$ measurements, the modification of the TDLAS instrument to use a dual optical path system, which compensates for order-of-magnitude differences in line intensities, may improve the precision of the instrument, because line pairs in the *P* or the *R* branch of the ν_3 band with much lower differences in their ground-state energies could then be used. The number of line-pair candidates would then also be larger, which would be advantageous if interferences from other gases were encountered in future field samples. Table 3 lists two possible line pairs (from the *R* branch). Further improvements to our methods may open the possibility of using the TDLAS instrument for background atmospheric CH_4 $\delta^{13}C$ measurements, which require a precision of approximately 0.1‰. However, both $\delta^{13}C$ and δD measurements of atmospheric CH_4 would require a preconcentration of CH_4, which one could perform by using charcoal at a temperature of 77 K.

We have demonstrated the capability of our TDLAS instrument for parallel $\delta^{13}C$ and δD measurements on CH_4 in samples from various natural and anthropogenic sources of atmospheric CH_4. The achieved overall $\delta^{13}C$ accuracy of 0.4–0.6‰ and overall δD accuracy of 5‰, as derived from the intercomparison with mass spectrometer measurements, is very satisfactory for investigations of atmospheric CH_4 sources, because the typical $\delta^{13}C$ and δD variabilities (e.g., temporal or spatial) in atmospheric CH_4 sources are distinctly larger. The advantage of the TDLAS instrument compared with the conventional MS is the ability to perform direct measurements on CH_4 samples without the need for any sample preparation (apart from drying) or for conversion of CH_4 to CO_2 and H_2. Currently the $\delta^{13}C$ or δD measurement of one sample requires 15 min, including the evacuation of the White cell and the automated filling of the sample. The subsequent zero measurement takes another 15 min. This short measurement time permits more comprehensive studies of $\delta^{13}C/\delta D$ variabilities[21] than have been practical in the past (especially in the case of δD measurements).

The δD precision for the TDLAS measurement, as derived from the comparision of TDLAS measurements at two different line pairs, is approximately the same as the reproducibility of MS measurements. Thus a fundamentally different measurement method for δD with essentially the same precision as the MS method is now available. Possible interferences, which may conceivably arise for certain kinds of field samples, may be avoided by choosing from the wide variety of $^{12}CH_3D/^{12}CH_4$ line pairs available.

We thank I. Levin for the permission to use her CH_4 sample preparation apparatus and K. Schweick-

hardt, who carried out some of the preparations for the $\delta^{13}C$ MS analysis. We also thank C. Junghans for her careful work in performing the MS analyses. We are grateful to E. Faber and E. Sohns for their δD (and additional $\delta^{13}C$) MS measurements. We also express our gratitude to L. R. Brown for providing us with her unpublished $^{12}CH_3D$ spectra, which initially greatly assisted us in identifying $^{12}CH_3D/^{12}CH_4$ line pairs.

References and Notes

1. R. A. Rasmussen and M. A. K. Khalil, "Atmospheric methane in the recent and ancient atmospheres: concentrations, trends, and interhemispheric gradient," J. Geophys. Res. **89,** 11599–11605 (1984).
2. D. R. Blake and F. S. Rowland, "Continuing worldwide increase in tropospheric methane, 1978 to 1987," Science **239,** 1129–1131 (1988).
3. D. M. Etheridge, G. I. Pearman, and P. J. Fraser, "Changes in tropospheric methane between 1841 and 1978 from a high accumulation-rate Antarctic ice core," Tellus **44,** 282–294 (1992).
4. J. Lelieveld, P. J. Crutzen, and C. Brühl, "Climate effects of atmospheric methane," Chemosphere **26,** 739–768 (1993).
5. R. J. Cicerone and R. S. Oremland, "Biogeochemical aspects of atmospheric methane," Global Biogeochem. Cycles **2,** 299–327 (1988).
6. C. M. Stevens and A. Engelkemeir, "Stable carbon isotopic composition of methane from natural and anthropogenic sources," J. Geophys. Res. **93,** 725–733 (1988).
7. M. Wahlen, N. Tanaka, R. Henry, B. Deck, J. Zeglen, J. S. Vogel, J. Southon, A. Shemesh, R. Fairbanks, and W. Broecker, "Carbon-14 in methane sources and in atmospheric methane: the contribution from fossil carbon," Science **245,** 286–290 (1989).
8. M. R. Manning, D. C. Lowe, W. Melhuish, R. Spaarks, G. Wallace, C. A. M. Brenninkmeijer, and R. C. McGill, "The use of radiocarbon measurements in atmospheric studies," Radiocarbon **32,** 37–58 (1990).
9. P. D. Quay, S. L. King, J. Stutsman, D. O. Wilbur, L. P. Steele, I. Fung, R. H. Gammon, T. A. Brown, G. W. Farwell, P. M. Grootes, and F. H. Schmidt, "Carbon isotopic composition of atmospheric CH_4: fossil and biomass burning source strengths," Global Biogeochem. Cycles **5,** 25–47 (1991).
10. S. C. Tyler, "The global methane budget," in *Microbial Production and Consumption of Greenhouse Gases: Methane, Nitrogen Oxides, and Halomethanes,* J. E. Rogers and W. B. Whitman, eds. (American Society for Microbiology, Washington, D.C., 1991), pp. 7–38.
11. Usually the stable isotope ratios are expressed in the δ notation

$$\delta = \left(\frac{R_{\text{sample}}}{R_{\text{standard}}} - 1\right)1000(‰),$$

where R_{sample}, R_{standard} are the $^{13}C/^{12}C$ (or D/H, i.e., $^2H/^1H$) ratios of the sample and a standard, respectively. Generally the PeeDee Belemnite (PDB) standard is used for $^{13}C/^{12}C$ ratios,[12] whereas D/H ratios are referenced to the standard mean ocean water (SMOW) standard.[13]
12. H. Craig, "Isotopic standards for carbon and oxygen and correction factors for mass-spectrometric analysis of carbon dioxide," Geochim. Cosmochim. Acta **12,** 133–149 (1957).
13. R. Hagemann, G. Nief, and E. Roth, "Absolute isotopic scale for deuterium analysis of natural waters, absolute D/H ratio for SMOW," Tellus **22,** 712–715 (1970).
14. M. J. Whiticar, E. Faber, and M. Schoell, "Biogenic methane formation in marine and freshwater environments: CO_2 reduction vs. acetate fermentation—isotope evidence," Geochim. Cosmochim. Acta **50,** 693–709 (1986).
15. M. Wahlen, "The global methane cycle," Ann. Rev. Earth Planet. Sci. **21,** 407–426 (1993).
16. R. A. Burke, T. R. Barber, and W. M. Sackett, "Seasonal variations of stable hydrogen and carbon isotope ratios of methane in subtropical freshwater sediments," Global Biogeochem. Cycles **6,** 125–138 (1992).
17. D. D. Coleman, J. B. Risatti, and M. Schoell, "Fractionation of carbon and hydrogen isotopes by methane-oxidizing bacteria," Geochim. Cosmochim. Acta **45,** 1033–1037 (1981).
18. R. A. Burke, T. R. Barber, and W. M. Sackett, "Methane flux and stable hydrogen and carbon isotope composition of sedimentary methane from the Florida Everglades," Global Biogeochem. Cycles **2,** 329–340 (1988).
19. M. J. Whiticar, "A geochemical perspective of natural gas and atmospheric methane," Org. Geochem. **16,** 531–547 (1990).
20. I. Levin, P. Bergamaschi, H. Dörr, and D. Trapp, "Stable isotopic signature of methane from major sources in Germany," Chemosphere **26,** 161–177 (1993).
21. P. Bergamaschi, "Messungen der $^{13}CH_4/^{12}CH_4$- und $^{12}CH_3D/^{12}CH_4$-Verhältnisse an Proben atmosphärischer Methanquellen mittels Diodenlaserabsorptionsspektrospkopie," Ph.D. dissertation (Universität Heidelberg, Heidelberg, Germany, 1993).
22. W. D. Hermichen and H. Schütze, "Zur Bedeutung der molekularen Diffusion für die Stoff- und Isotopentrennung bei der Bildung und Zerstörung von Erdgaslagerstätten," Isotopenpraxis **23,** 285–289 (1987).
23. E. J. Mroz, "Deuteromethanes: potential fingerprints of the sources of atmospheric methane," Chemosphere **26,** 45–53 (1993).
24. R. Bösinger, "Isotopenmessungen an atmosphärischem und quellnahem Methan," Ph.D. dissertation (Universität Heidelberg, Heidelberg, Germany, 1990).
25. D. C. Lowe and C. A. M. Brenninkmeijer, "Determination of the isotopic composition of atmospheric methane and its application in the Antarctic," J. Geophys. Res. **96,** 15455–15467 (1991).
26. I. Dumke, E. Faber, and J. Poggenburg, "Determination of stable carbon and hydrogen isotopes of light hydrocarbons," Anal. Chem. **61,** 2149–2154 (1989).
27. C. R. Webster and R. D. May, "*In situ* stratospheric measurements of CH_4, $^{13}CH_4$, N_2O, and $OC^{18}O$ using the BLISS tunable diode laser spectrometer," Geophys. Res. Lett. **19,** 45–48 (1992).
28. W. W. Wong, "Comparison of infrared and mass-spectrometric measurements of carbon-13/carbon-12 ratios," Int. J. Appl. Radiat. Isot. **36,** 997–999 (1985).
29. J. F. Becker, T. B. Sauke, and M. Loewenstein, "Stable isotope analysis using diode laser spectroscopy," Appl. Opt. **31,** 1921–1927 (1992).
30. M. Wahlen and T. Yoshinari, "Oxygen isotope ratios in N_2O from different environments," Nature (London) **313,** 780–782 (1985).
31. P. S. Lee and R. F. Majkowski, "High resolution infrared diode laser spectroscopy for isotope analysis—measurement of isotopic carbon monoxide," Appl. Phys. Lett. **48,** 619–621 (1986).
32. S. M. Anderson, J. Morton, and K. Mauersberger, "Laboratory measurements of ozone isotopomers by tunable diode laser absorption spectroscopy," Chem. Phys. Lett. **156,** 175–180 (1989).
33. M. Schupp, P. Bergamaschi, G. W. Harris, and P. J. Crutzen, "Development of a tunable diode laser absorption spectrometer for measurements of the $^{13}C/^{12}C$ ratio in methane," Chemosphere **26,** 13–22 (1993).

34. M. Schupp, "Entwicklung und Demonstration einer laserspektroskopischen Methode zur Messung des Kohlenstoffisotopenverhältnisses in Methan," Ph.D. dissertation (Universität Mainz, Mainz, Germany, 1992).
35. M. Schupp, P. Bergamaschi, and G. W. Harris, "Measurements of the $^{13}C/^{12}C$ ratio in methane using a tunable diode laser absorption spectrometer," in *Monitoring of Gaseous Pollutants by Tunable Diode Lasers,* R. Grisar, H. Böttner, M. Tacke, and G. Restelli, eds. (Kluwer, Dordrecht, The Netherlands, 1992), pp. 343–352.
36. A. Fried, B. Henry, and J. R. Drummond, "Tunable diode laser ratio measurements of atmospheric constituents by employing dual fitting analysis and jump scanning," Appl. Opt. **32,** 821–827 (1993).
37. C. R. Webster, R. T. Menzies, and E. D. Hinkley, "Infrared laser absorption: theory and applications," in *Laser Remote Chemical Analysis,* R. M. Measures, ed. (Wiley, New York, 1988), pp. 163–272.
38. The subscript indicates the measurement method: mass spectrometry (MS) or TDLAS; the superscript indicates the scale to which the δ values are referred (PDB, SMOW, reference). The measured gas (sample, reference, calibration) is identified within the parentheses.
39. L. S. Rothman, R. R. Gamache, R. H. Tipping, C. P. Rinsland, M. A. H. Smith, D. Chris Benner, V. Malathy Devi, J.-M. Flaud, C. Camy-Peyret, A. Perrin, A. Goldman, S. T. Massie, L. R. Brown, and R. A. Toth, "The HITRAN molecular database: editions of 1991 and 1992," J. Quant. Spectrosc. Radiat. Transfer **48,** 469–507 (1992).
40. R. A. Toth, L. R. Brown, R. H. Hunt, and L. S. Rothman, "Line parameters of methane from 2385 to 3200 cm^{-1}," Appl. Opt. **20,** 932–935 (1981).
41. We define the mean deviation $\Delta\delta\ ^{13}C$ ($\Delta\delta D$) as

$$\Delta\delta = \left\{\frac{1}{n}\sum_{i=1}^{n}\left[\delta_{MS}(i) - \delta_{TDLAS}(i)\right]^2\right\}^{1/2}.$$

This provides a better measure of the comparison than the slopes and intercepts of the regression lines, which in all cases were insignificantly different from unity and zero.
42. L. S. Rothman, R. R. Gamache, A. Goldman, L. R. Brown, R. A. Toth, H. M. Pickett, R. L. Poynter, J.-M. Flaud, C. Camy-Peyret, A. Barbe, N. Husson, C. P. Rinsland, and M. A. H. Smith, "The HITRAN database: 1986 edition," Appl. Opt. **26,** 4058–4097 (1987).